Apr 1963
Vine
Copy 2

EXPERIMENTAL STRESS ANALYSIS OF A MODEL OF THE ALVIN HULL

D. J. Bynum
R. C. DeHart

Final Report
3 April 1963

SwRI Project No. 1206-3
P. O. No. ED 25316

DOCUMENT
LIBRARY
Woods Hole Oceanographic
Institution

Prepared for

General Mills Electronics Group
2003 East Hennepin Avenue
Minneapolis 13, Minnesota

Attn: Mr. H. E. Froehlich

SOUTHWEST RESEARCH INSTITUTE
SAN ANTONIO, TEXAS

VM
163
.B9
1963
c.1

SOUTHWEST RESEARCH INSTITUTE
8500 Culebra Road, San Antonio 6, Texas

Department of Structural Research

EXPERIMENTAL STRESS ANALYSIS OF A MODEL OF THE ALVIN HULL

D. J. Bynum
R. C. DeHart

Final Report
3 April 1963

SwRI Project No. 1206-3
P. O. No. ED 25316

Prepared for

General Mills Electronics Group
2003 East Hennepin Avenue
Minneapolis 13, Minnesota

Attn: Mr. H. E. Froehlich

APPROVED:

Robert C DeHart
Robert C. DeHart, Director
Department of Structural
Research

MBL/WHOI
0 0301 0043051 8

SOUTHWEST RESEARCH INSTITUTE
8500 Culebra Road, San Antonio 6, Texas

EXPERIMENTAL STRESS ANALYSIS OF A MODEL OF THE ALVIN HULL

SwRI Project No. 1206-3

for

General Mills, Inc. - P. O. No. ED-25316
Electronics Division - 2003 E. Hennepin
Minneapolis 13, Minnesota

Under Contract (P. O. 18284) with
Woods Hole Oceanographic Institution
Woods Hole, Massachusetts

Funded under Prime Contract Nonr 3484(00) with:

The Office of Naval Research
Department of the Navy
Code 466 - Washington 25, D. C.

Prepared by: D. J. Bynum
R. C. DeHart

Approved by: Dr. Robert C. DeHart, Director
Department of Structural Research

3 April 1963

EPITOME

A model of the hull of Alvin was subjected to loads of uniform external pressures, and the resultant stress distribution was experimentally determined. The model was basically a "thin" hemispherical shell having a thickened portion at the window opening. The study also included an analysis of the effect of cable penetrations in the thickened portion of the shell. The results from the experimental stress analysis can be transformed by structural similitude to verify the adequacy of the full scale design.

NOMENCLATURE

Symbol		Units
a	Inside radius	in.
b	Outside radius	in.
p_i	Internal Pressure	psi
p_o	External Pressure	psi
μ	Poisson's ratio	numeric
E	Young's modulus of elasticity	psi
σ_{cr}, σ_e	Buckling stress, and endurance stress, respectively	psi
σ_y, σ_u, τ_u	Tensile yield strength, ultimate tensile strength and shear strength, respectively	psi
α	Span angle of a simply supported portion of a sphere	degrees
σ_m, σ_h, σ_b	Meridional stress, hoop stress, and boundary stress, respectively	psi
GF	Strain gage factor	numeric
CF	Ratio of gage factor used divided by true gage factor	numeric
R	Resistance	ohms
C	Constant	numeric
x	Distance from specimen centerline of symmetry to centerline of strain gage, measured along concave or convex surface of specimen	in.
θ	Angular location, measured counterclockwise on convex surface	degrees

TABLE OF CONTENTS

Page

EPITOME ii

NOMENCLATURE iii

I. INTRODUCTION 1

II. MATERIAL PROPERTIES 3

III. THEORETICAL STRESSES 5

IV. TEST PROCEDURE 8

V. DISCUSSION OF RESULTS 12

- A. Results for Configuration A 12
- B. Results for Configuration B 12
- C. General Comments 14
- D. Accuracy of Results 15

VI. CONCLUSIONS 16

ACKNOWLEDGMENTS 17

REFERENCES 18

LIST OF ILLUSTRATIONS 20

LIFT OF TABLES 34

APPENDIX A. EPISTEMOLOGY OF THE BIREFRINGENT COATING TECHNIQUE 47

- 1. History of the Birefringent Coating Technique 47
- 2. Principles of the Birefringent Coating Analysis 48
- 3. Advantages of a Birefringent Coating Analysis 51

I. INTRODUCTION

The work described herein covers the experimental stress analysis of a 0.286 scale, hemispherical model which was subjected to loads of uniform external pressures. The model simulated the hull of an oceanographic vessel being designed and fabricated by the General Mills Company for the Woods Hole Oceanographic Institution. The full scale design has been referred to as "Alvin" by the above two organizations. The results from the experimental stress analysis of the scaled model can be transformed by structural similitude to verify the adequacy of the full scale design.

Tests were conducted with two configurations of the model, the cross sections of which are given in Figure 1. Both model configurations had a plexiglass window. Dr. J. W. Mavor* and Mr. F. Pons** are shown in Figure 2 checking the thickness variation of Configuration A by utilizing a granite flat (flat within 0.0001") and a mechanical displacement type of gage. All dimensions were found to be well within the specified tolerances given in Figure 1.

After the test with the pristine configuration was completed, the port was machined to the larger diameter, as shown in Figure 1, and a

---

* Engineer, Woods Hole Oceanographic Institution, Woods Hole, Massachusetts

** Machinist, Machine Shop, Southwest Research Institute

larger window was fabricated for the test of Configuration B. Through holes simulating cable penetrations and half-through holes simulating bolt holes were also machined in Configuration B, as shown in Figure 3. The cable penetrations and the half-through holes were drilled parallel with the through holes directed to the center of the 11.373 radius of the concave model surface (Fig. 1).

The cable penetrations were sealed with plugs having 0.005" clearance with the hole walls and specially made "O" rings (Fig. 4). Since strain gages were installed at the edge of the holes, the plugs were welded to brackets which overspanned the holes. The ends of the bracket legs were ground to fit the contour of the model, and the "O" rings were located at the half-thickness of the shell wall with the plugs in place.

II. MATERIAL PROPERTIES

The formed hemispherical head was made from 7079-T6 aluminum, and was machined to the final dimensions of Configuration A by the Hahn and Clay Machine and Boiler Works*. Typical mechanical properties of this material are as follows(1)**:

σ_u = 77 ksi

σ_y = 66 ksi

Elongation in 2" = 4% minimum

Brinell hardness number = 150, (500 kg load, 10 mm ball)

τ_u = 48 ksi

σ_e = 22 ksi, (Based on 5×10^8 cycles of reversed stress)

E = 10.4×10^6 psi

A Poisson's ratio of 0.33 was used in the stress computations for the aluminum.

The plexiglass*** port had the following mechanical properties(2):

Tensile Strength	ASTM D-638-46T, 1/4" specimen (0.2"/min)	7 ksi
Flexural Strength	ASTM D-790-45T, Span-depth ratio of 16(0.1"/min)	12 ksi
Compressive Strength	ASTM D-695-44T (0.2"/min)	12 ksi

---

* 5100 Clinton Drive, Houston 20, Texas

** Superscripts in parenthesis pertain to the references given at the conclusion of the text

*** Trade name of a methyl acrylate; available from the Rohm and Haas Co., Washington Square, Philadelphia 5, Pa.

A Young's modulus of elasticity of 400 ksi and a Poisson's ratio of 0.5 were used in the stress computations for the plastic.

III. THEORETICAL STRESSES

The Lamé equations$^{(3)}$ for the stresses in thick-walled spheres are:

$$\sigma_m = \frac{p_o b^3(2R^3 + a^3)}{2R^3(a^3 - b^3)} - \frac{p_i a^3(2R^3 + b^3)}{2R^3(a^3 - b^3)}$$

$$\sigma_r = \frac{p_o b^3(R^3 - a^3)}{R^3(a^3 - b^3)} + \frac{p_i a^3(b^3 - R^3)}{R^3(a^3 - b^3)}$$

$$\sigma_h = \sigma_m$$

Since the internal pressure was zero,

$$\frac{\sigma_m}{p_o} = \frac{b^3(2R^3 + a^3)}{2R^3(a^3 - b^3)}$$

$$\frac{\sigma_r}{p_o} = \frac{b^3(R^3 - a^3)}{R^3(a^3 - b^3)}$$

On the concave side of the head

$$\frac{\sigma_m}{p_o} = 15.9 \text{ psi/psi}$$

$$\frac{\sigma_r}{p_o} = 0$$

On the convex side of the head

$$\frac{\sigma_m}{p_o} = 15.4 \text{ psi/psi}$$

$$\frac{\sigma_r}{p_o} = -1 \text{ psi/psi}$$

The small difference in the magnitudes of the stresses on the concave and convex surfaces of the head indicate that the head should be considered as a thin shell. Using thin shell theory, the membrane stress per unit of external pressure load was

$$\frac{\sigma}{p} = \frac{r}{2t} = \frac{11.373}{2(0.381)} = 14.9 \text{ psi/psi}$$

The critical buckling stress(4) is:

$$\sigma_{cr} = \frac{Et}{r(1-\mu^2)} \left[\left(\frac{1-\mu^2}{3} \right)^{1/2} - \frac{\mu t}{2r} \right]$$

$$= \frac{(10.4 \times 10^6)(0.381)}{11.373(1-0.33^2)} \left[\left(\frac{1-0.33^2}{3} \right)^{1/2} - \frac{0.33(0.381)}{2(11.373)} \right]$$

$$= 212 \text{ ksi}$$

The critical buckling stress given by this equation varies between 3 and 4 times as much higher than that found by experiment. Using a factor of three, the resultant shell stresses rather than buckling considerations are shown to govern the strength of the hemisphere.

The following empirical relationship can be used to determine the buckling pressure in the given limits:

$$p_{cr} = 0.3E \left[\frac{t}{r} \right]^2 \left[1 - 0.175 \left(\frac{\alpha - 20}{20} \right) \right] \left[1 - \frac{0.07\, r}{400\, t} \right]$$

when

$$400 \leq \frac{r}{t} \leq 2000$$

and

$$20° \leq \alpha \leq 60°$$

The geometry of the model tested was not within these limits of applicability.

Considering the allowable shear through to be one-half of the tensile yield strength, the allowable pressure on the plexiglass window from the standpoint of shear stress was:

$$p_o = \frac{2t\tau}{r} = \frac{t\sigma}{r} = \frac{1.00(7000)}{0.537} = 13,000 \text{ psi}$$

IV. TEST PROCEDURE

Electrical resistance type of strain gages were used to measure the strains produced by the external pressure applied to the hemispherical model. Detailed information on the various types of gages used are given in Table 1. Rectangular rosettes of the gages were installed on the concave and convex side of the head in a manner so that for any particular rosette, a corresponding rosette was located on the opposite surface on a radial line drawn from the center of curvature of the concave surface. A row of rosettes was installed across the meridian, $\theta = 0°$, with the θ orientation as given in Figure 3, and at $\theta = 90°$ in order to ascertain the degree of symmetrical response of the vessel.

Figure 5 shows the strain gages being installed by Mr. E. J. Winkler, a technician in the Structural Research Department. The complete strain gage installations for Configuration A, on the concave and convex surfaces are shown in Figures 6 and 7, respectively. The complete strain gage installations for Configuration B on the concave and convex surfaces are shown in Figures 8 and 9, respectively. Two of the seal plugs for the cable penetrations are shown in place in the close-up view (Fig. 10). The wires to the gages on the convex surfaces were brought through the vessel in three Conax fittings (Fig. 6).

The test setup is shown in Figure 11 being prepared by Messieurs E. J. Winkler and J. J. Jones, technicians in the Structural Research Department. A paper gasket with sealing compound was placed between the lid of the pressure facility and the model to effect a seal. The model was held to the lid of the pressure facility (Fig. 11) by means of a turnbuckle bar (Figs. 7,and 9) until the initial seal between the lid and model was formed. The bar was then loosened before beginning the tests.

End blocks on the bar were bonded with epoxy to the shell with the test setup of Configuration A. This arrangement proved unsatisfactory so small indentations were made in the model to hold the bar (Fig. 9) for the test of Configuration B.

The edge of the port window was coated with sealing compound and taped in place for the tests of Configuration A. A small amount of oil seeped between the window and the head until the initial seal was reached. In order to eliminate leakage, the window was bonded to the shell with Duco cement for the tests of Configuration B.

A Gilmore Strain Gage Plotter (Fig. 11) was used to record the strains in the model. The model was cycled between 100 and 1, 600 psi external pressure several times in order to stabilize the strain gage installations, and then the strains were recorded at each increment of 300 psi from 100 to 1, 600 psi, and finally again at 100 psi. For convenience during the tests

the Gilmore was set for a gage factor of 2.04. The corrected strain was found by applying a faciend to the indicated strain since

$$\epsilon_{true} = \frac{\Delta R}{R(GF)_{true}}$$

$$\epsilon_{indicated} = \frac{\Delta R}{R(GF)_{set}}$$

$$\epsilon_{corrected} = \epsilon_{indicated}\left(\frac{GF_{set}}{GF_{true}}\right) = \epsilon_{indicated}(CF)$$

The stresses were then computed using the plane stress relations

$$\sigma_m = \frac{E}{1-\mu^2}(\epsilon_m + \mu\epsilon_h)$$

$$\sigma_h = \frac{E}{1-\mu^2}(\epsilon_h + \mu\epsilon_m)$$

Since the radial stress is zero at a free boundary, the stress at the boundaries of the cable penetrations were computed using the relation

$$\sigma_b = E\epsilon$$

The pressure effects on the type of gages used in this study have been found to be negligible at the low pressures(5). To insure that the applied pressure would not effect the indicated strains, compensation gages were placed on blocks of the same material as the shell and the port window, and the gages on these blocks (Fig. 6) were subjected to atmospheric pressure and to the applied external pressure during the test for compensation of the gages on the concave and convex surfaces of the shell, respectively.

The usual three-wire lead hook-up self-temperature compensating gages could not be used since the Gilmore Strain Gage Plotter requires a dummy gage in the circuit. The urgent need for the results necessitated the use of SwRI stock strain gages, and since insufficient aluminum compensated gages were available, some steel compensated gages were used. Consequently, one of each of these two types of gages was installed on the aluminum dummy blocks inside and outside of the pressure facility and appropriately wired into the circuits.

V. DISCUSSION OF RESULTS

A. Results for Configuration A

The strain data and stress results are given in Tables 2 through 7, and the normalized stress distribution and variation of shell thickness are plotted in Figure 12. This graphical representation of the stress distribution is self-explanatory, and the membrane stresses are shown to be the highest stresses in the structure. The average experimentally determined membrane stress per unit load of 15.5 psi/psi can be compared to the theoretical membrane stress of 14.9 psi/psi.

B. Results for Configuration B

The strain data and stress results are given in Tables 8 through 12, and the normalized stress distribution across meridians (not coincident with the cable penetrations) is given in Figure 13. The membrane stress on these meridians were again of larger magnitude than in the vicinity of the port, and the average membrane stress was of about the same magnitude as for Configuration A.

The boundary stresses about the simulated cable penetrations and bolt holes are given in Tables 11 and 12, with strain gage locations as given in Figure 3. Insufficient data was obtained around the circumference of these discontinuities to obtain meaningful, graphical representations; however, the gages were located such that the given results provide the significant data necessary for design purposes.

The stress concentration factors for the two sizes of cable penetrations without bolt holes based on the theoretical membrane stress were 1.28 for the 0.358" diameter hole, and 0.97 for the 0.144" diameter hole. The location of the maximum stress for each of these two sizes of holes was on the concave surfaces at the hole boundary on the penetration centerline circle. These factors are comparable to the theoretical factor of 2 for an infinite plate of uniform thickness with a hole, subjected to a biaxial stress field(6).

The stress concentration factors for the two sizes of cable penetrations with bolt holes, again based on the theoretical membrane stress, were 1.21 for the 0.358" diameter hole, and 1.03 for the 0.144" diameter hole. The location of these maximum stresses corresponded to the locations of maximum stress for the cable penetrations without bolt holes.

The stresses around the bolt holes near the 0.358" diameter cable penetration were greater than those near the 0.144" diameter, and the stresses around the bolt holes for either case were less than that at any of the cable penetrations. The bolt hole boundaries were at the same distance from the boundaries of the cable penetrations for both sizes of the penetrations. The stress concentration factors for the cable penetrations decrease directly as a function of the ligament efficiency, i.e., the stress intensity decreases as the distance between the penetration and the bolt holes decreases.

C. General Comments

Some question may be raised as to the effect of the plug arrangement for sealing the cable penetrations. The pressure acting on the hole walls between the convex surface and the "O" ring seal can easily be shown to have a negligible effect on the overall or local stress distribution, intensity, or direction.

The 0.005" clearance provided between the plug and the hole wall was demonstrated in the Gilmore strain plot to be adequate. The strain-pressure plots for the gages around each hole were linear, but the plots would have been nonlinear with the occurrence of binding between the plugs and the perforation walls.

Note should be made of the fact that since the reported stresses were computed using measurements from strain gages which have a definite gage length, the stresses as given are the integrated stresses over that gage length, and not the stress at a point. Also, to have installed the gages with the gage centerline at the boundaries of the discontinuities was physically impossible and the actual locations are given in the tables. Comparing the reported results with experience in this area of experimental stress analysis, the true stress at a point on the boundaries of the discontinuitities could be as much as 35% higher than the stresses reported herein.

In the absence of flexural stresses, the theoretical stress per unit load at the penetration boundary would be 15.8 psi/psi, based on a stress

concentration factor of 2 applied to the theoretical membrane stress, considering the shell thickness at the hole boundary. The experimental stresses given in Tables 11 and 12 vary between 20% greater and 66% less than the theoretical value.

If a more accurate determination of stress at the boundaries of the discontinuities is required the birefringent coating technique should be used since the stresses could be obtained exactly at the hole boundary. Also, the individual principal stresses could be obtained from measurements of relative retardation with normal and oblique incidence without any integration effect since the specimen was symmetrical. A description of the birefringent coating technique is given in the Appendix for the interested reader.

D. Accuracy of Results

The accuracy of any reported results are as important as the results themselves. The maximum deviation of the results reported in these tests from the true stresses is estimated to be ±4% maximum, neglecting the integration effect over the gage length and the small distance between the gage centerline and the boundaries of the discontinuities.

VI. CONCLUSIONS

The following conclusions can be drawn:

(1) The maximum stress in the Configuration A model was the membrane stress, and this stress was almost equal to the theoretical membrane stress.

(2) The maximum stress in the Configuration B model, except at the cable penetrations, was the membrane stress, and this stress was of about the same intensity as that with Configuration A.

(3) The cable penetrations caused a stress of higher magnitude than the membrane stress, with the higher stress concentration factor for the larger size of hole.

(4) The stress concentration factor at the cable penetration was decreased when bolt holes were used, and decreased further for the case of the bolt holes located closer to the cable penetration.

(5) The magnitude of the stresses at the boundaries of the bolt holes was less than the membrane stress.

ACKNOWLEDGMENTS

Installation of the strain gages and the operation of the recording system was ably performed by Messrs. E. J. Winkler and J. J. Jones, and their competence and diligent efforts during the conduct of the tests deserve special note.

LIST OF REFERENCES

1. Alcoa Aluminum Handbook, 1959, Aluminum Co. of America, Pittsburgh, Pa., p. 72.

2. Modern Plastics Encyclopedia, Vol. 35, No. 1A, Sept. 1957, 575 Madison Ave., New York 22, N. Y., pp. 83, 315.

3. Timoshenko, S., and Goodier, J. N., Theory of Elasticity, 2nd Ed., McGraw-Hill Book Co., 1951, p. 359.

4. Timoshenko, S. P., and Gere, J. M., Theory of Elastic Stability, 2nd Ed., McGraw-Hill Book Co., 1961, p. 517-19.

5. Gerdeen, J. C., "Effects of Pressure on Small Foil Strain Gages," Exp. Mech., Vol. 3, No. 3, Mar. 1963,pp. 73-80.

6. Peterson, R. E., Stress Concentration Design Factors, 1953, John Wiley & Sons, Inc., New York, p. 93.

7. Mesnager, A. "Sur la détermination optique des tensions intérieures dans des solides à trois dimensions." Comptes Rendus, Paris, V. 190, 1930, p. 1249.

8. Mabboux, Georges, " Applications de la photoélasticimetre a l'étude des ouvrages en béton, " Revue d'Optique, V. II, 1932, pp. 501-507.

9. Oppel, G., "Das polarizationsoptische Schichtverfahren zur Messung der Oberflächenspannung am beanspruchten Bauteil ohne Modell," Vereines Deutscher Ingenieure, Zeitschrift, V. 81, 1937, pp. 803-804.

10. D'Agostino, J., Drucker, D. C., Liu, C. K., and Mylonas, "An Analysis of Plastic Behavior of Metals with Bonded Birefringent Plastic," Proceed. SESA, V. XII, No. 2, 1955, pp. 115-122.

11. Zandman, F., Photostress, Principles and Applications, Budd Co., P. O. Box 245, Phoenixville, Pa.

12. Coker, E. G., Filon, L. N. G., and Jessop, H. T., A Treatise on Photo-Elasticity, 2nd Ed., Cambridge Univ. Press, 32 East 57th St., New York 22, N. Y., 1957.

13. Frocht, M. M., Photoelasticity, John Wiley and Sons, Inc., New York, N. Y., V. 1, 1941.

14. Flügge, S., Editor, Elasticity and Plasticity, Encyclopedia of Physics, V. 6, Springer-Verlag, Berlin, 1958.

15. Bynum, D. J., and Lemcoe, M. M., "Birefringent Coating Analysis of Laterally Loaded Perforated Plates," Soc. Exp. Stress Anal., Paper No. 767.

16. Bynum, D. J., and Lemcoe, M. M., "Stresses and Deflections in Laterally Loaded Perforated Plates," WRC Bul. 80, Aug. 1962, Welding Research Council, 345 E. 47th St., New York 17, N. Y.

17. "Photostress Conversion Table," Bulletin IB8023, Budd Company, P. O. Box 245, Phoenixville, Pa, 30 Jan. 1959.

18. Hetényi, M., Editor, Handbook of Experimental Stress Analysis, John Wiley and Sons, Inc., New York, N. Y., p. 863.

19. Bynum, D. J., "Birefringent Coating Analysis of a Tensile Plate Containing a Heterogeneous Inclusion, Utilizing Fringe Multiplication," M. S. Thesis, University of Washington, 1961.

20. Bynum, D. J., "Combined Stresses in Curved Beams," Soc. Exp. Stress Anal., Paper No. 815.

21. Day, E. E., Kobayashi, A. S., and Larson, C. N., "Fringe Multiplication and Thickness Effects in Birefringent Coating," Exp. Mech., Vol. 2, No. 4, Apr. 1962, pp. 115-122.

22. Bynum, D. J., "Fillet and Groove Stress Concentrations," Soc. Exp. Stress Anal., Paper No. 777.

LIST OF ILLUSTRATIONS

Figure

1 Cross-Section of Models

2 Hemispherical Model, Configuration A

3 Details of Configuration B

4 Seal Plugs for Cable Penetrations

5 Strain Gage Installation

6 Complete Strain Gage Installation on Convex Surface, Configuration A

7 Complete Strain Gage Installation on Concave Surface, Configuration A

8 Complete Strain Gage Installation on Convex Surface, Configuration B

9 Complete Strain Gage Installation on Concave Surface, Configuration B

10 Close-Up View of Strain Gage Installation, Configuration B

11 Test Setup

12 Normalized Stress Distribution and Variation of Shell Thickness, Configuration A

13 Normalized Stress Distribution and Variation of Shell Thickness, Configuration B

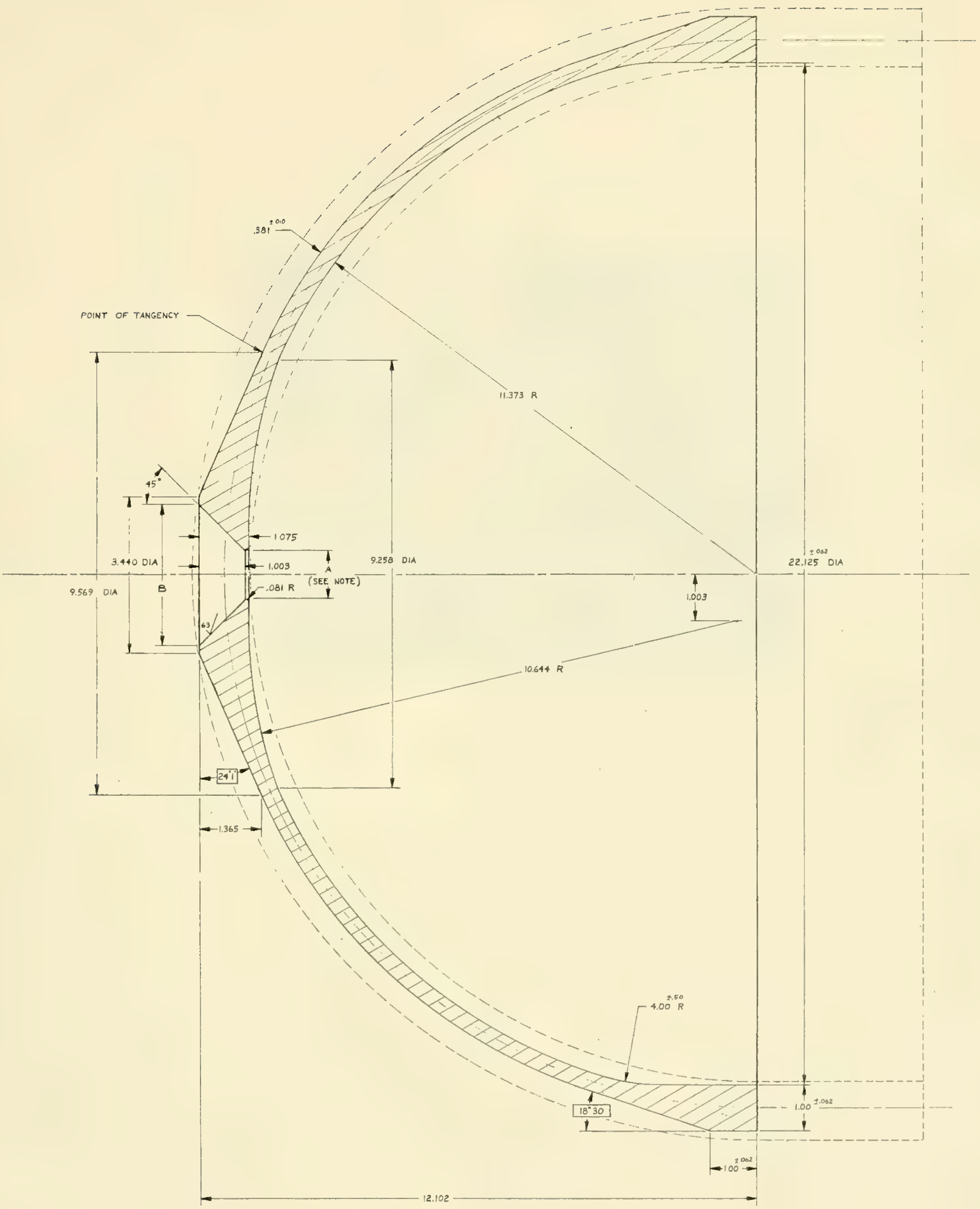

NOTE:

1-

TEST NO.	DIM. A	DIM. B (REF)
1	1.075	3.082
2	1.434	3.440

2- 125 FINISH ALL OVER

UNLESS OTHERWISE SPECIFIED DIMENSIONS ARE IN INCHES
TOLERANCES ON DECIMALS ANGLES
±.015 ±15'
MATERIAL
ORIGINAL DATE OF DRAWING MARCH 1, 1963
DRAWN K.H.KUBE
ENGINEER E d H.
CHECKED E L N
APPROVED HE7
General Mills ELECTRONICS DIVISION MINNEAPOLIS MINNESOTA
.2867 MODEL TEST SPHERE
CODE IDENT NO 98731
SIZE E
542005
SCALE 1-1
SHEET

-FIGURE I CROSS-SECTION OF MODELS

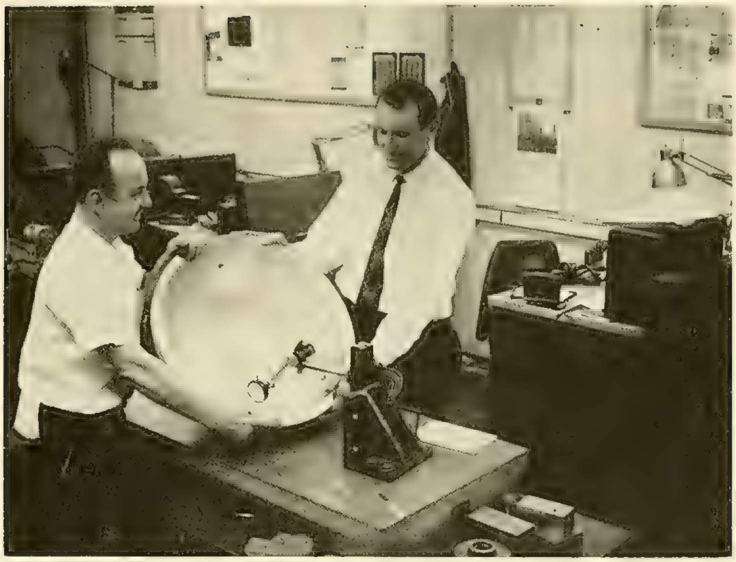

FIGURE 2. HEMISPHERICAL MODEL, CONFIGURATION A

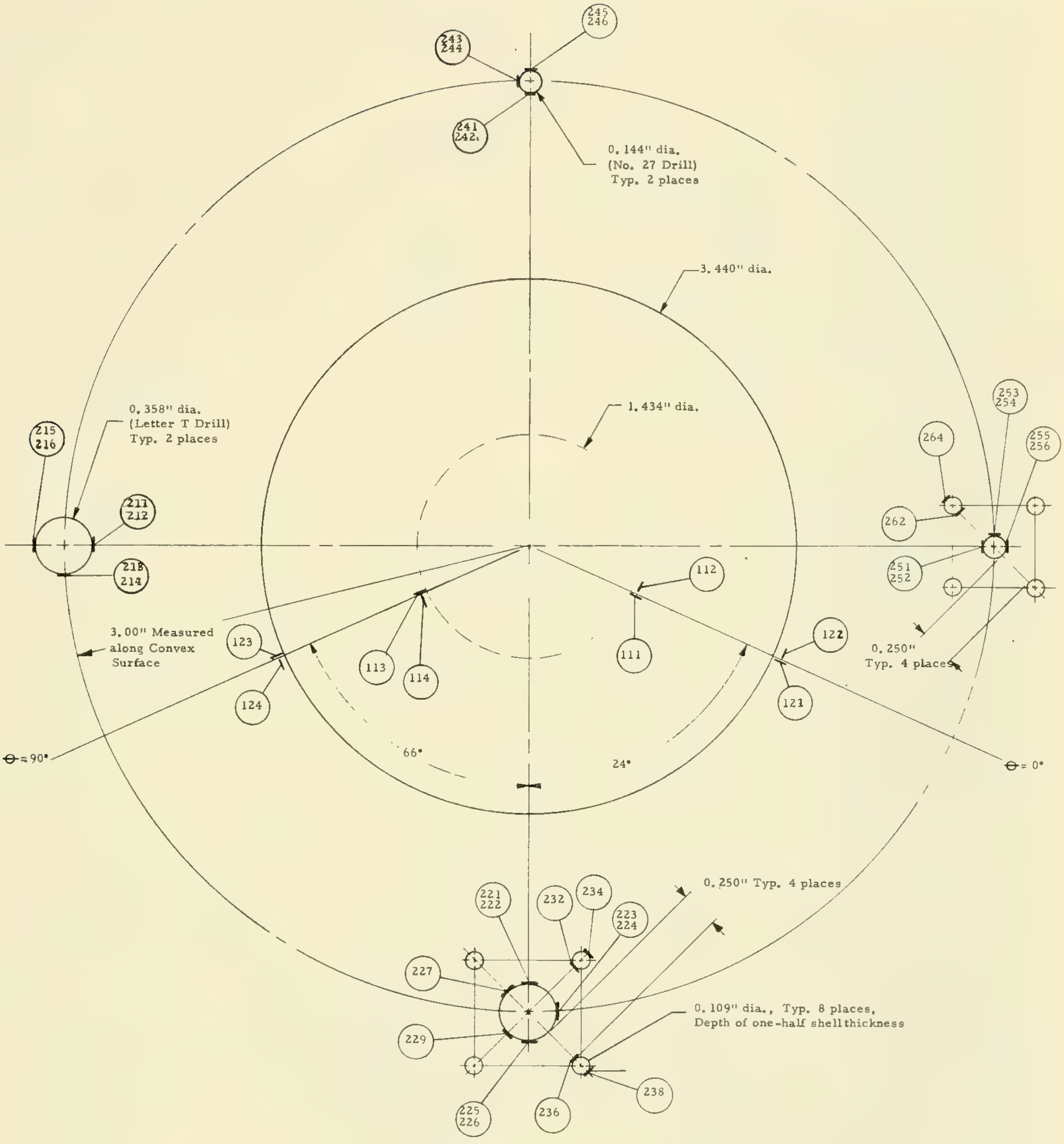

NOTE: STRAIN GAGE NUMBERS ARE CIRCLED

FIGURE 3. DETAILS OF CONFIGURATION B

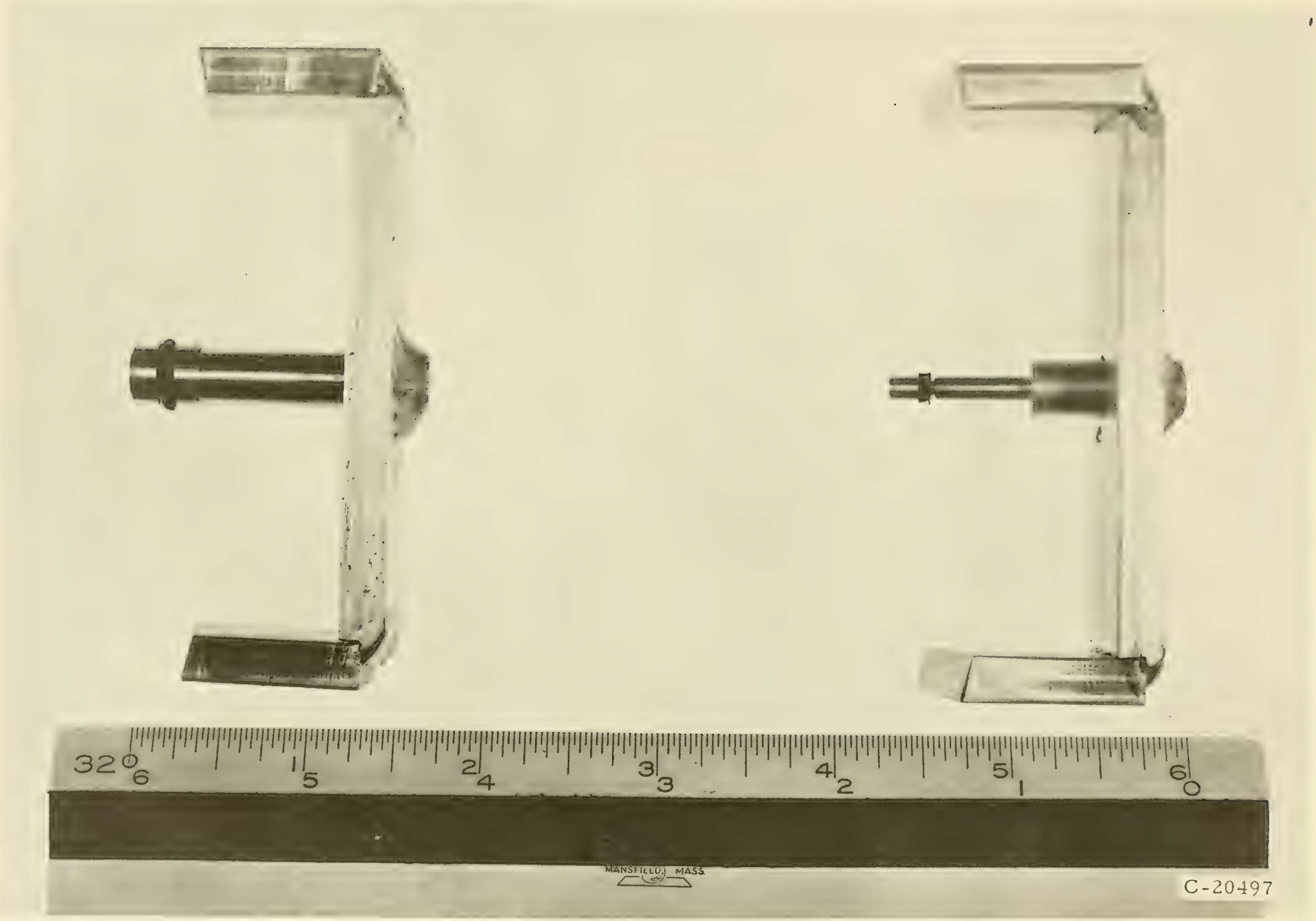

FIGURE 4. SEAL PLUGS FOR CABLE PENETRATIONS

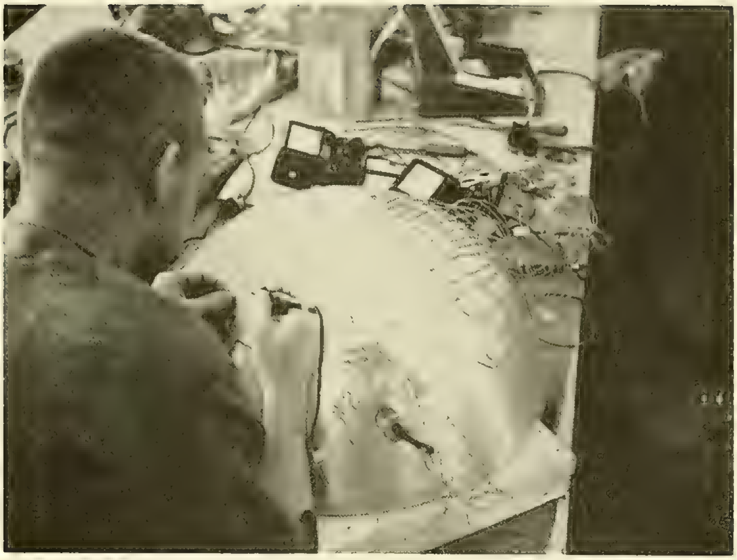

FIGURE 5. STRAIN GAGE INSTALLATION

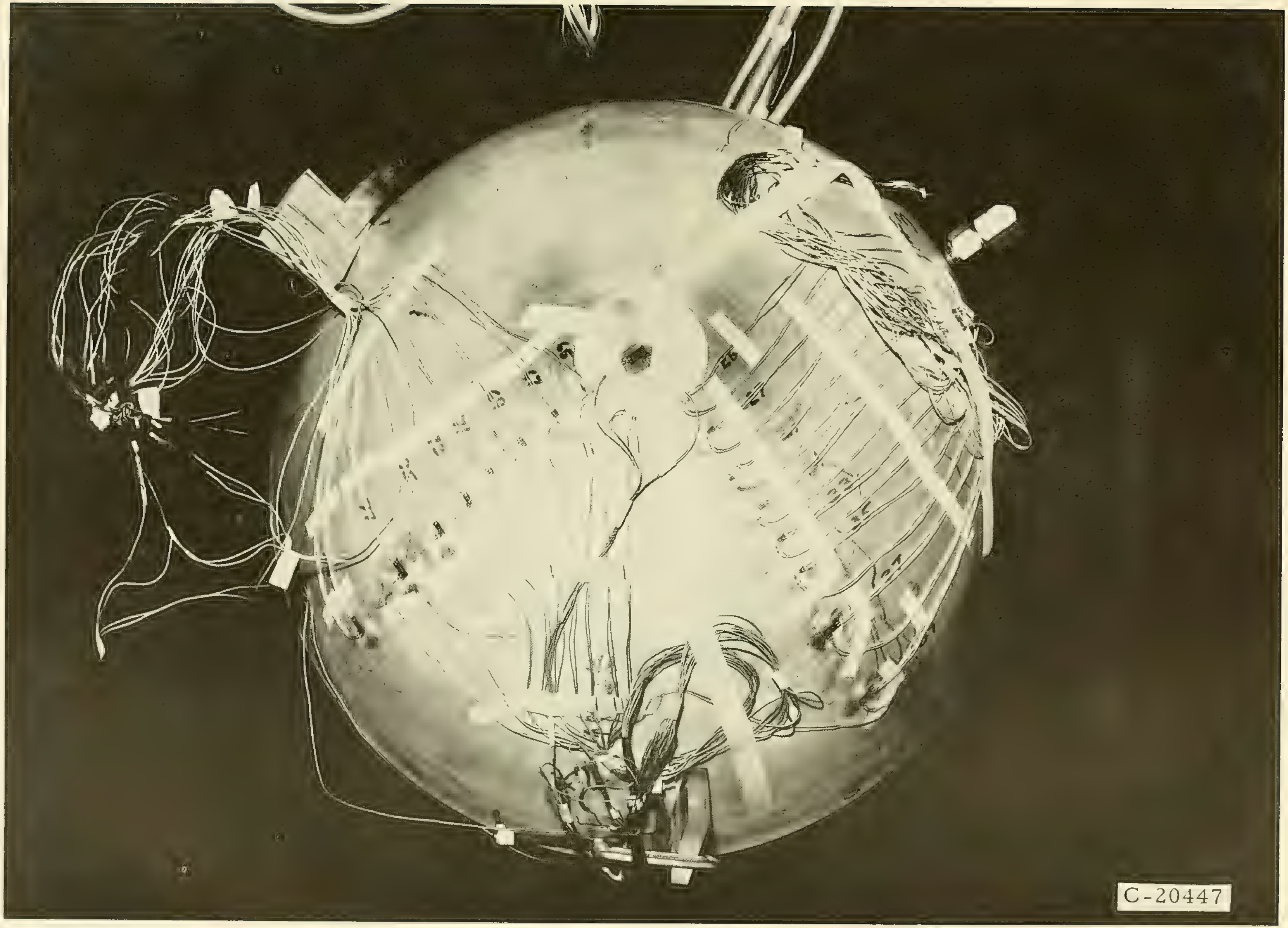

FIGURE 6. COMPLETE STRAIN GAGE INSTALLATION ON CONVEX SURFACE, CONFIGURATION A

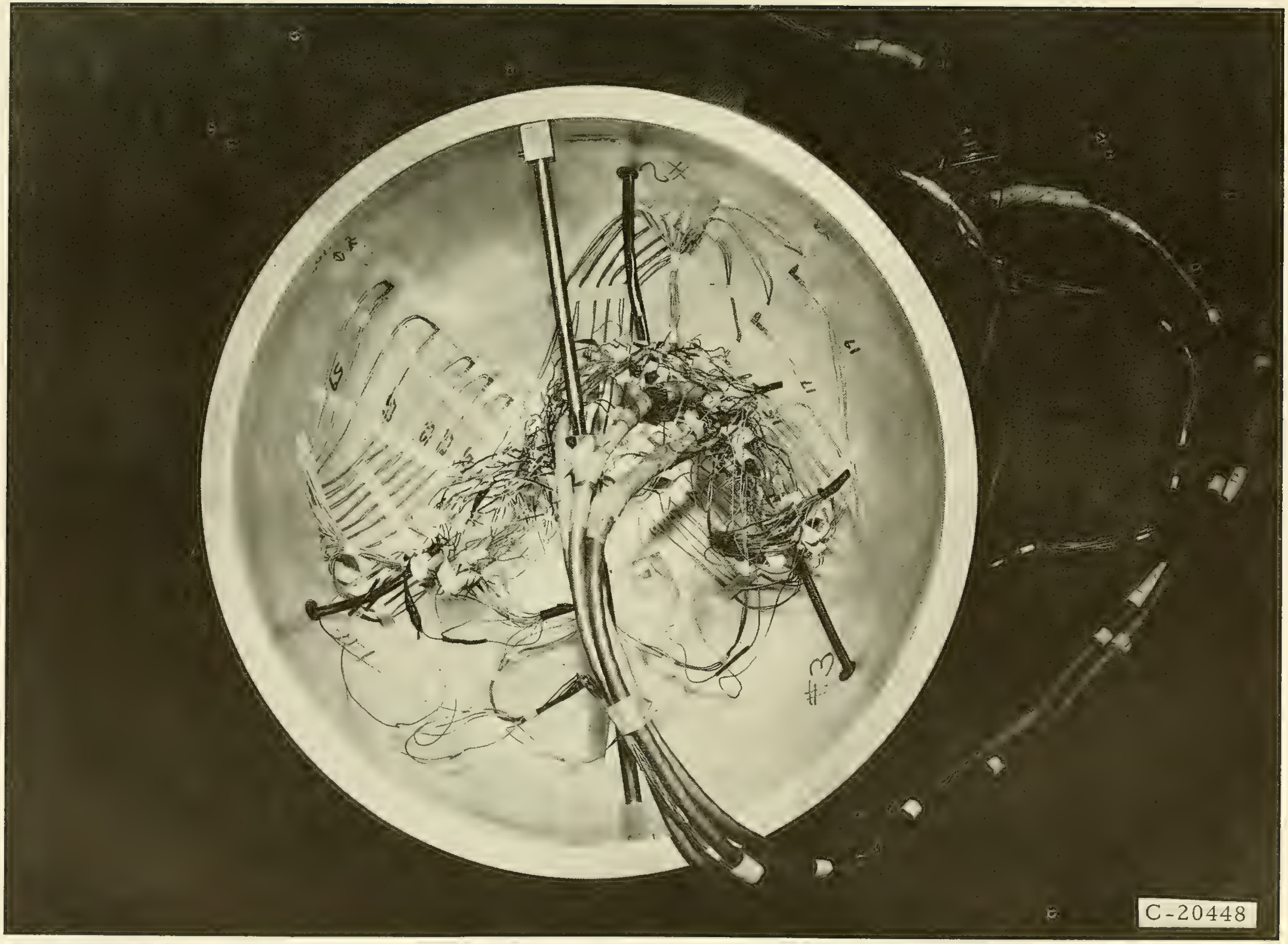

FIGURE 7. COMPLETE STRAIN GAGE INSTALLATION ON CONCAVE SURFACE, CONFIGURATION A

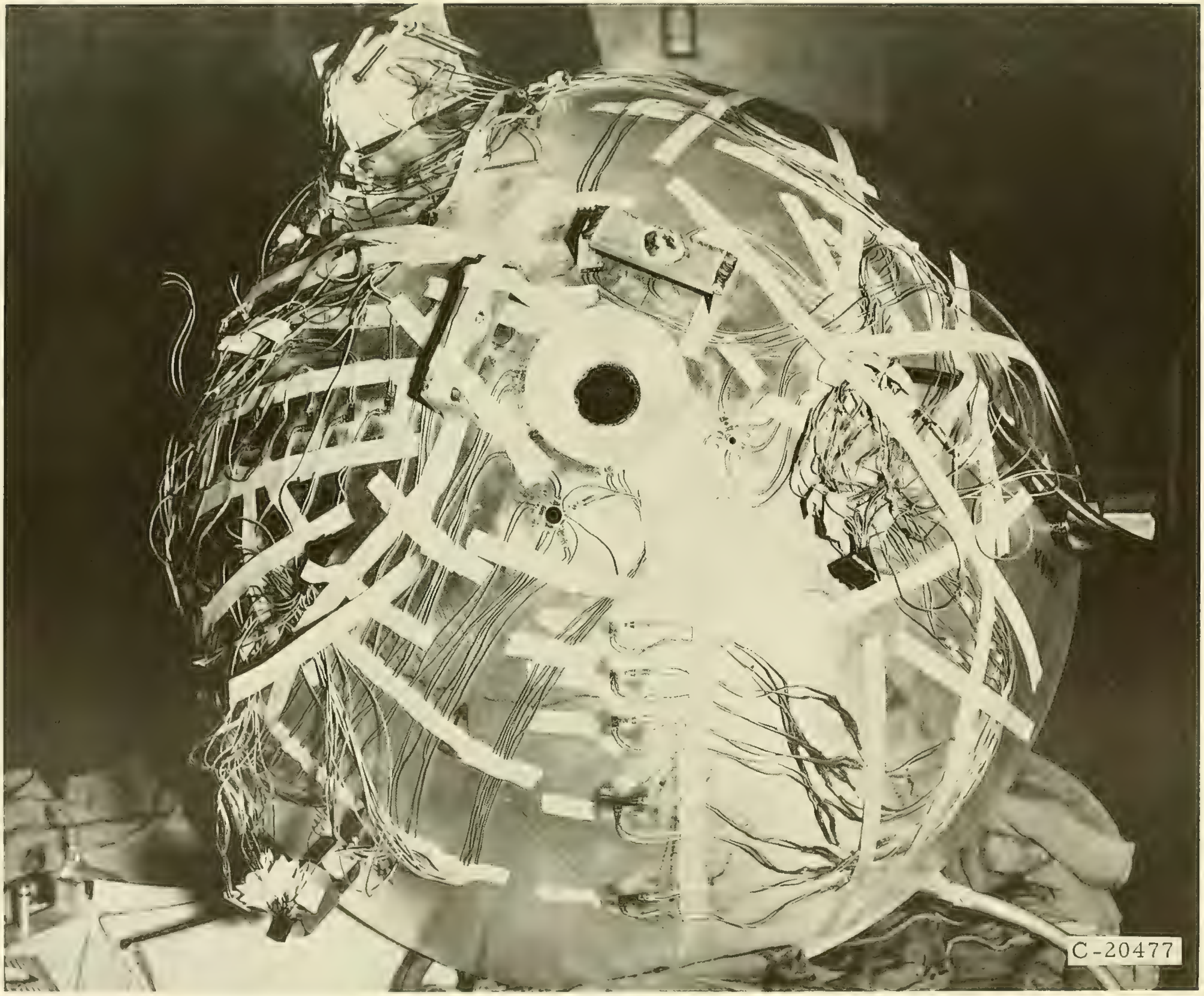

FIGURE 8. COMPLETE STRAIN GAGE INSTALLATION ON CONVEX SURFACE, CONFIGURATION B

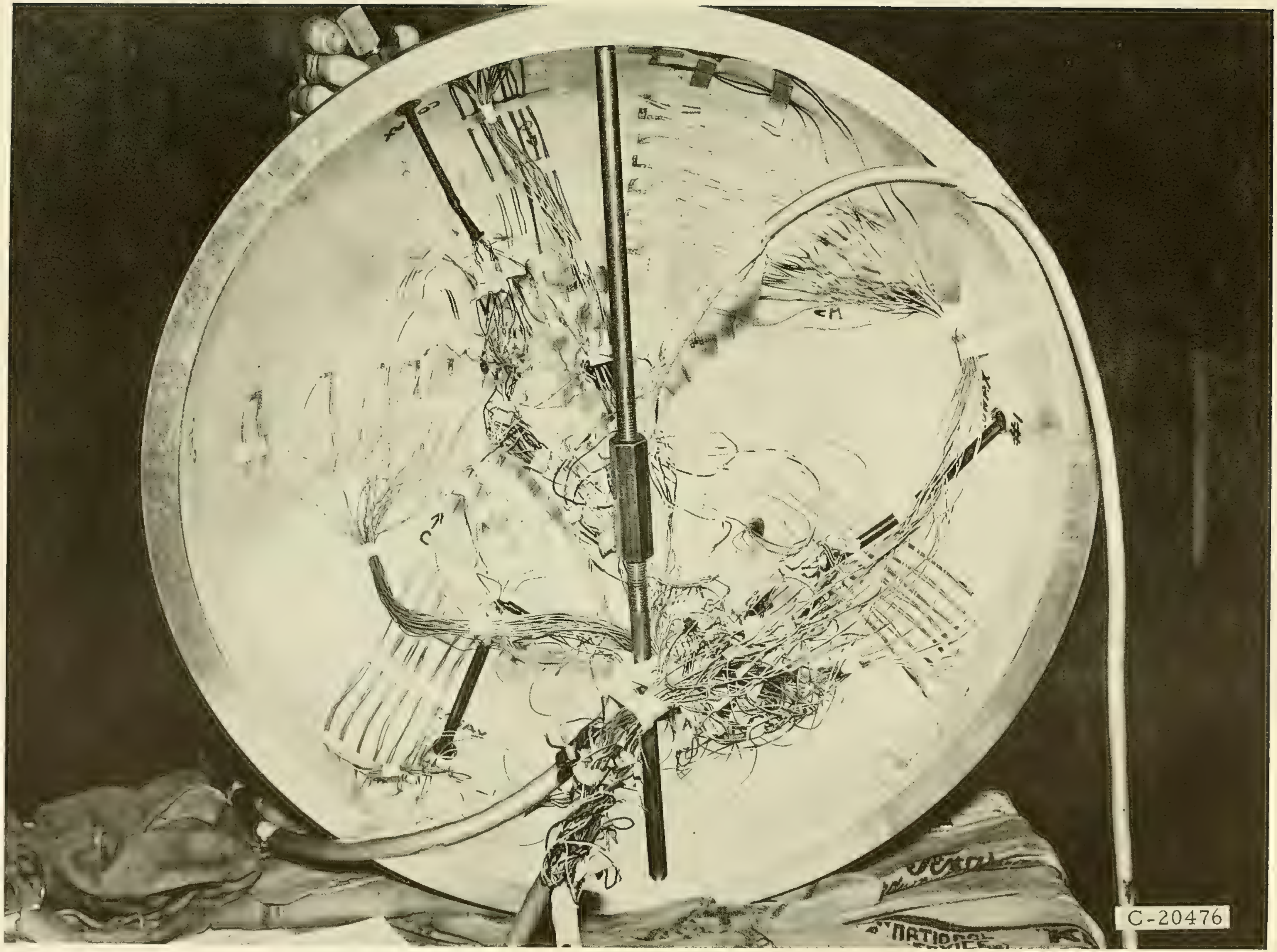

FIGURE 9. COMPLETE STRAIN GAGE INSTALLATION ON CONCAVE SURFACE, CONFIGURATION B

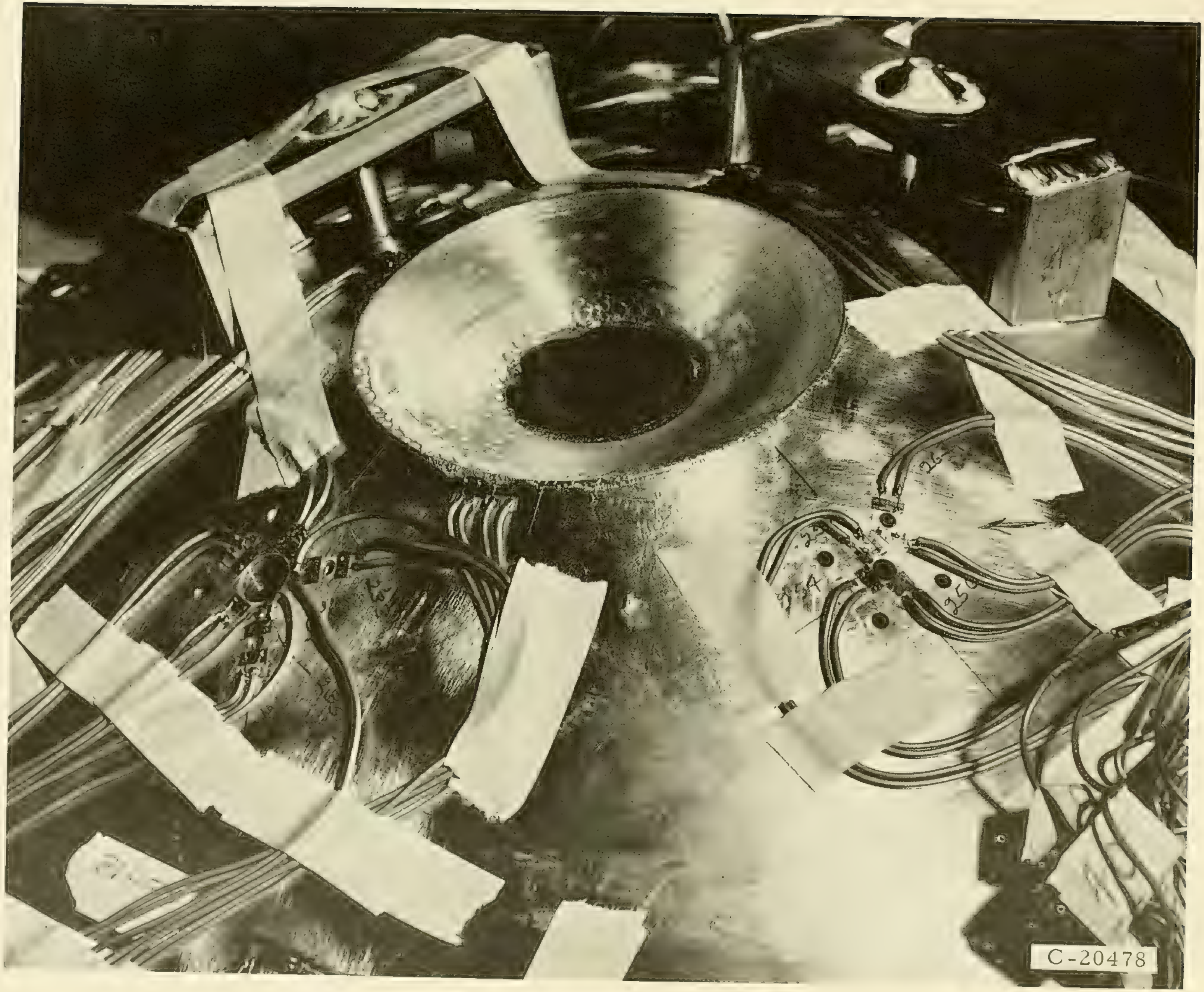

FIGURE 10. CLOSE-UP VIEW OF STRAIN GAGE INSTALLATION, CONFIGURATION B

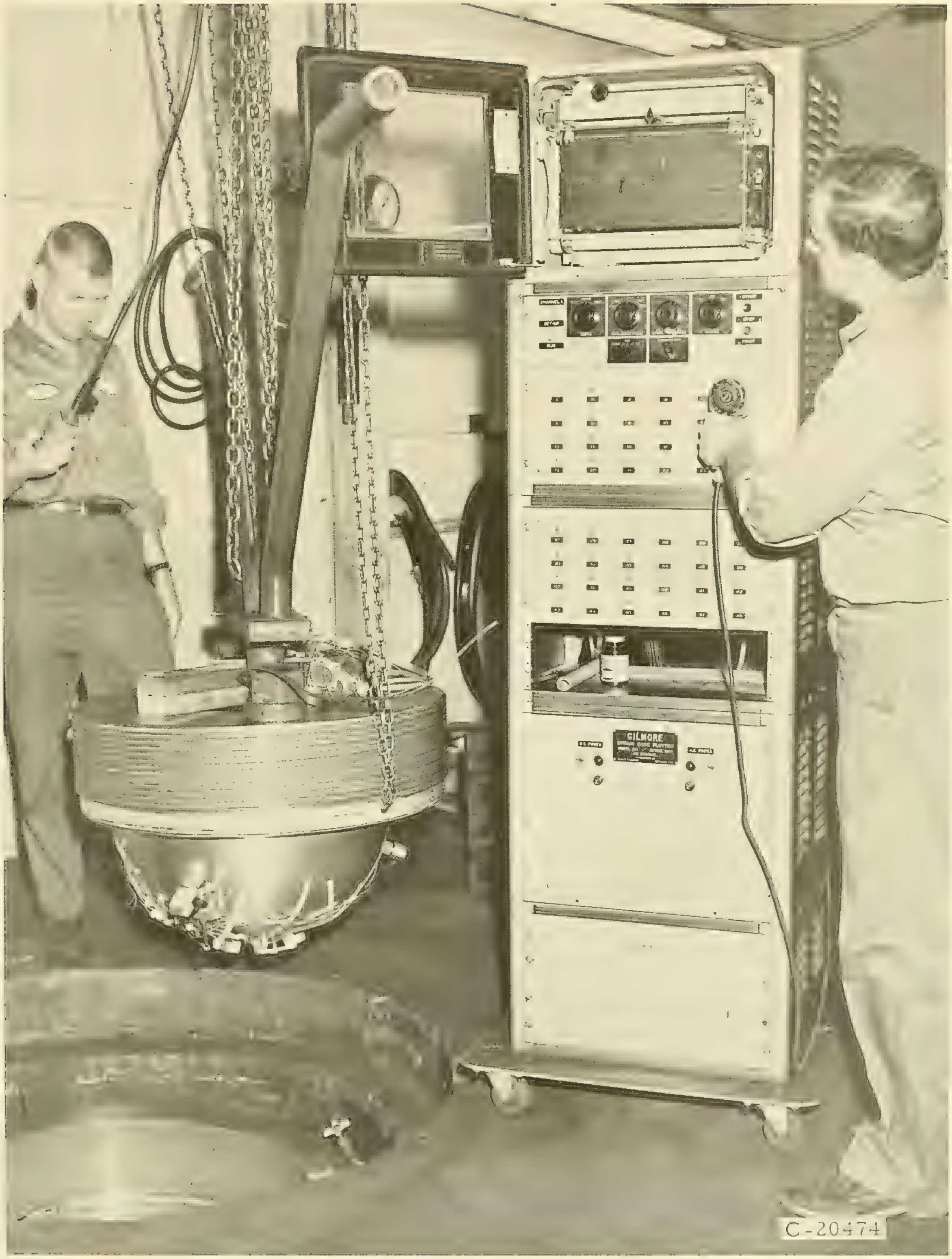

FIGURE 11. TEST SETUP

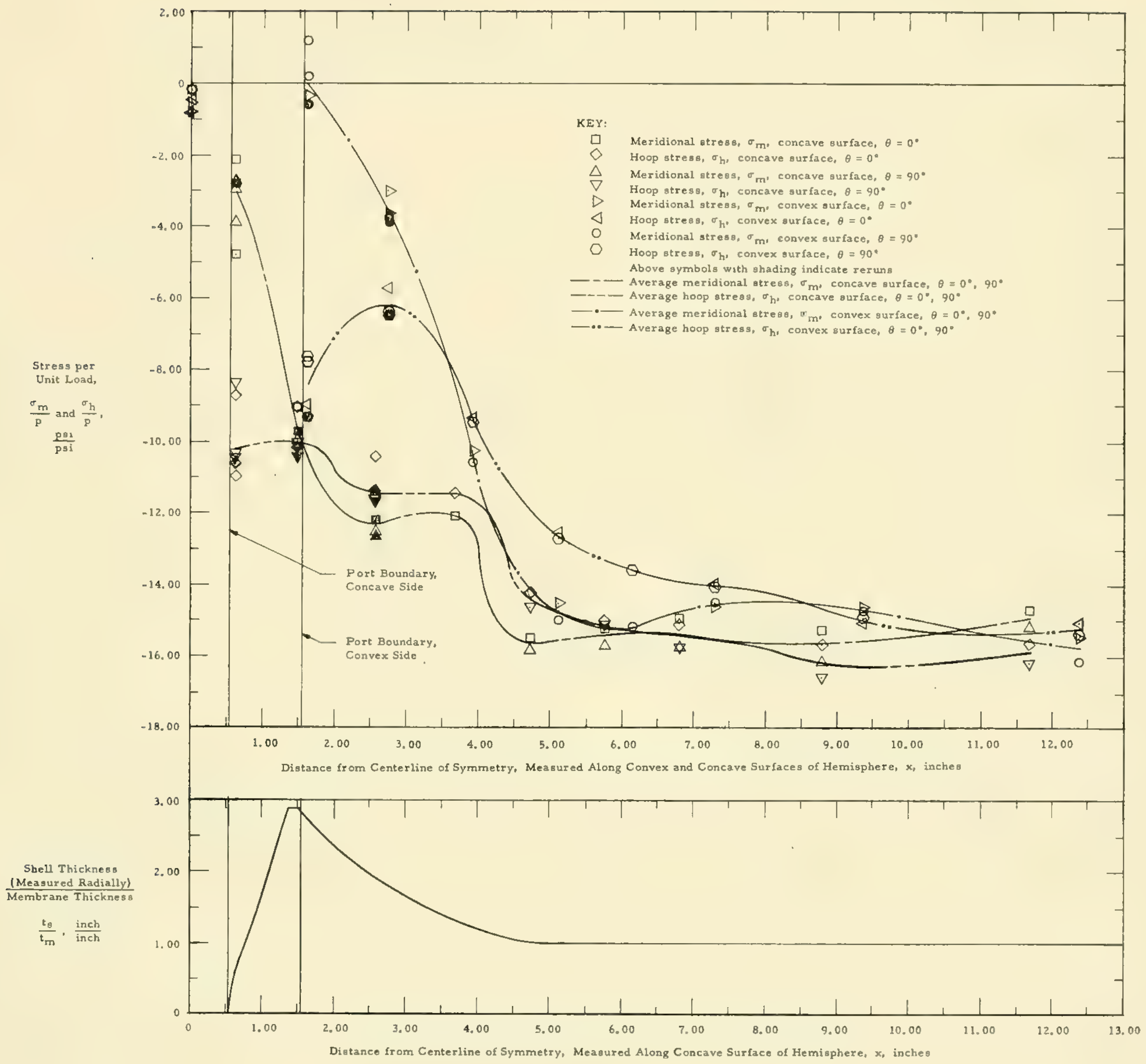

FIGURE 12. NORMALIZED STRESS DISTRIBUTION AND VARIATION OF SHELL THICKNESS, CONFIGURATION A

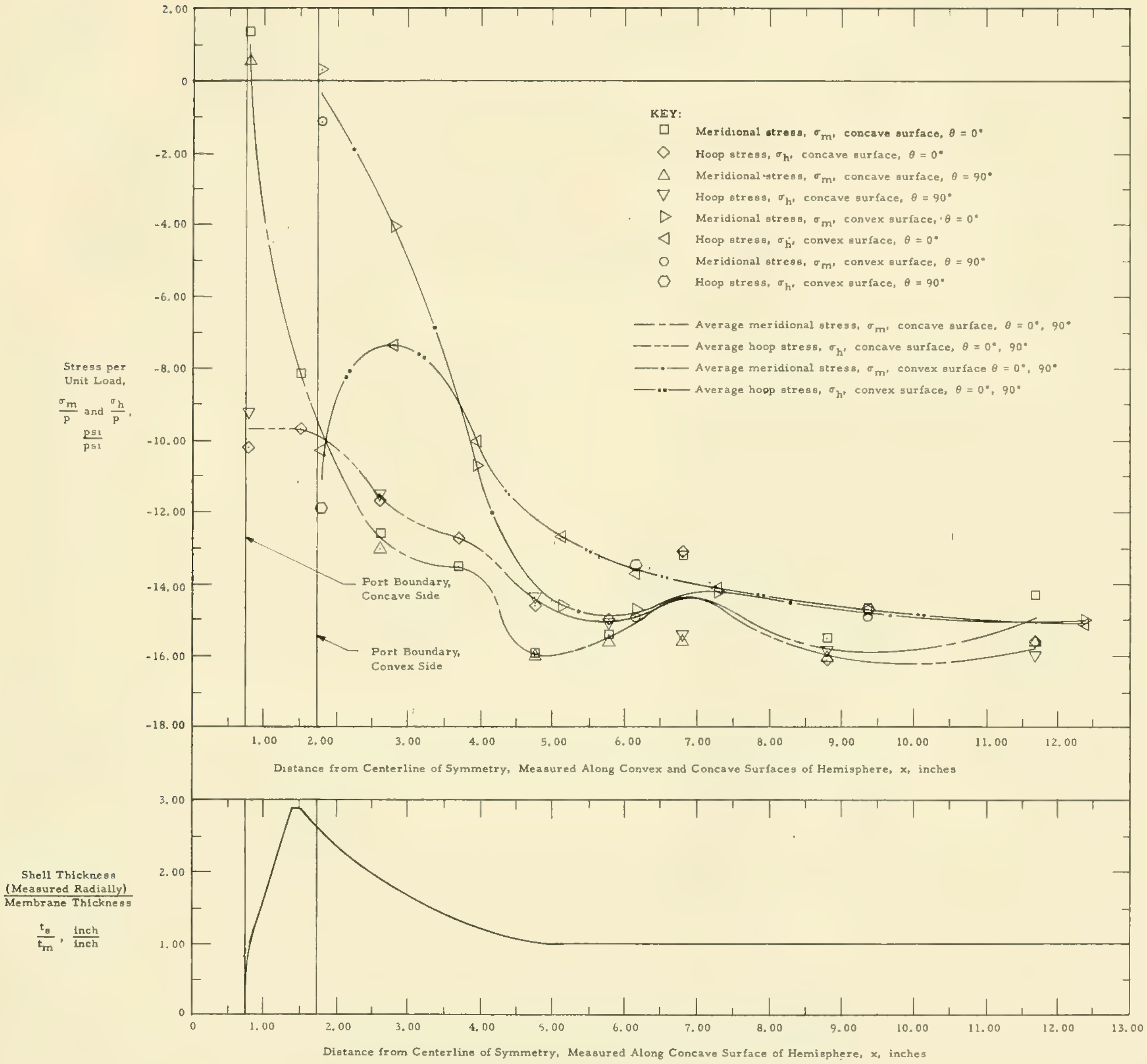

FIGURE 13. NORMALIZED STRESS DISTRIBUTION AND VARIATION OF SHELL THICKNESS, CONFIGURATION B

LIST OF TABLES

Table

1 Characteristics of Strain Gages Used

2 Strain Gage Data and Results, Configuration A, Concave Surface, $\theta = 0°$

3 Strain Gage Data and Results, Configuration A, Convex Surface, $\theta = 0°$

4 Strain Gage Data and Results, Configuration A, Concave Surface, $\theta = 90°$

5 Strain Gage Data and Results, Configuration A, Convex Surface, $\theta = 90°$

6 Strain Gage Data and Results for Additional Gages at Port Boundary, Configuration A

7 Strain Gage Data and Results, Configuration A, Reruns

8 Strain Gage Data and Results, Configuration B, $\theta = 0°$

9 Strain Gage Data and Results, Configuration B, $\theta = 90°$

10 Strain Gage Data and Results for Gages at Port Boundary, Configuration B

11 Strain Gage Data and Results for Gages at Boundaries of Cable Penetrations without Bolt Holes, Configuration B

12 Strain Gage Data and Results for Gages at Boundaries of Cable Penetrations and Bolt Holes, Configuration B

TABLE 1. CHARACTERISTICS OF STRAIN GAGES USED

Strain Gage Type Number	Manufacturer's Strain Gage Number	Gage Length, inches	Electrical Resistance, R, ohms	Gage Factor, GF	Correction Factor, CF
1	C12-1X1-64*	1/64	120 ± 1	1.83 ± 3%	1.114
2	C12-111*	1/16	120 ± 0.5	2.04 ± 1%	1
3	C6-111*	1/16	120 ± 0.5	2.01 ± 1%	1.015
4	C6-121*	1/8	120 ± 0.2	2.07 ± 0.5%	0.985
5	C6-121*	1/8	120 ± 0.2	2.02 ± 0.5%	1.010
6	EA-13-031DE-120**	1/32	120 ± 0.4	2.07 ± 1%	0.985
7	EA-13-031EC-120**	1/32	120 ± 0.4	2.01 ± 1%	1.015

---

* Available from Budd Co., P. O. Box 245, Phoenixville, Pa.

** Available from Micro-Measurements, Inc., 38905 Chase Road, Romulus, Michigan.

TABLE 2. STRAIN GAGE DATA AND RESULTS, CONFIGURATION A, CONCAVE SURFACE, $\theta = 0°$

Strain Gage Number*	Strain Gage Type	Correction Factor, CF	Corrected Strain, ϵ, μ-in./in., (at p = 1500 psi)	Meridional Stress per Unit Load, $\frac{\sigma_m}{p}$, $\frac{psi}{psi}$	Hoop Stress per Unit Load, $\frac{\sigma_h}{p}$, $\frac{psi}{psi}$	Distance**, x, inches
1***	5	1.010	-465	-0.21		0
2***	5	1.010	-384		-0.19	0
5	2	1	-880	-9.09		1.50
6	2	1	-880		-9.09	1.50
7	2	1	-1160	-11.5		2.59
8	2	1	-960		-10.4	2.59
9	2	1	-1200	-12.1		3.69
10	2	1	-1080		-11.5	3.69
11	2	1	-1560	-15.5		4.75
12	2	1	-1320		-14.3	4.75
13	3	1.015	-1480	-15.2		5.78
14	3	1.015	-1440		-15.0	5.78
15	3	1.015	-1440	-15.0		6.81
16	3	1.015	-1460		-15.1	6.81
17	4	0.985	-1460	-15.3		8.81
18	4	0.985	-1540		-15.7	8.81
19	4	0.985	-1380	-14.7		11.69
20	4	0.985	-1560		-15.6	11.69

---

* Odd numbered gages were installed in meridional direction, and even numbered gages were installed in circumferential direction.

** Distance from centerline of port to center of strain gage, measured along concave surface of hemisphere.

*** Gages applied to plexiglass window.

TABLE 3. STRAIN GAGE DATA AND RESULTS, CONFIGURATION A, CONVEX SURFACE, $\theta = 0°$

Strain Gage Number*	Strain Gage Type	Correction Factor, CF	Corrected Strain, ϵ, μ-in./in., (at p = 1500 psi)	Meridional Stress per Unit Load, $\frac{\sigma_m}{p}$, $\frac{psi}{psi}$	Hoop Stress per Unit Load, $\frac{\sigma_h}{p}$, $\frac{psi}{psi}$	Distance**, x, inches
21***	5	1.010	-1210	-0.53		0
22***	5	1.010	-889		-0.46	0
27	2	1	-160	-2.99		2.78
28	2	1	-680		-5.69	2.78
29	2	1	-1040	-10.3		3.94
30	2	1	-860		-9.34	3.94
31	2	1	-1500	-14.5		5.13
32	2	1	-1120		-12.5	5.13
33	3	1.015	-	-		6.16
34	3	1.015	-1260		-	6.16
35	3	1.015	-1440	-14.6		7.31
36	3	1.015	-1320		-14.0	7.31
37	4	0.985	-1400	-14.7		9.38
38	4	0.985	-1480		-15.1	9.38
39	4	0.985	-1520	-15.5		12.38
40	5	1.010	-1430		-15.0	12.38

---

* Odd numbered gages were installed in meridional direction, and even numbered gages were installed in circumferential direction.

** Distance from centerline of port to center of strain gage, measured along convex surface of hemisphere.

*** Gages applied to plexiglass window.

TABLE 4. STRAIN GAGE DATA AND RESULTS, CONFIGURATION A, CONCAVE SURFACE, $\theta = 90°$

Strain Gage Number*	Strain Gage Type	Correction Factor, CF	Corrected Strain, ϵ, μ-in./in., (at p = 1500 psi)	Meridional Stress per Unit Load, $\frac{\sigma_m}{p}$, $\frac{psi}{psi}$	Hoop Stress per Unit Load, $\frac{\sigma_h}{p}$, $\frac{psi}{psi}$	Distance**, x, inches
43	1	1.114	-156	-3.84		0.63
44	1	1.114	-1020		-8.36	0.63
45	2	1	-960	-9.97		1.50
46	2	1	-980		-10.1	1.50
47	2	1	-1260	-12.6		2.59
48	2	1	-1080		-11.6	2.59
49	2	1	-1260	-		3.69
50	2	1	-		-	3.69
51	3	1.015	-1580	-15.8		4.75
52	3	1.015	-1360		-14.6	4.75
53	3	1.015	-1540	-15.7		5.78
54	3	1.015	-1440		-15.2	5.78
55	3	1.015	-1520	-15.7		6.81
56	3	1.015	-1520		-15.7	6.81
57	3	1.015	-1540	-16.2		8.81
58	3	1.015	-1630		-16.6	8.81
59	5	1.010	-1410	-15.1		11.69
60	5	1.010	-1620		-16.2	11.69

---

* Odd numbered gages were installed in meridional direction, and even numbered gages were installed in circumferential direction.

** Distance from centerline of port to center of strain gage, measured along concave surface of hemisphere.

TABLE 5. STRAIN GAGE DATA AND RESULTS, CONFIGURATION A, CONVEX SURFACE, $\theta = 90°$

Strain Gage Number *	Strain Gage Type	Correction Factor, CF	Corrected Strain, ϵ, μ-in./in., (at p = 1500 psi)	Meridional Stress per Unit Load, $\frac{\sigma_m}{p}$, $\frac{psi}{psi}$	Hoop Stress per Unit Load, $\frac{\sigma_h}{p}$, $\frac{psi}{psi}$	Distance**, x, inches
65	1	1.114	535	1.18		1.63
66	1	1.114	-1160		-7.63	1.63
67	2	1	-240	-3.76		2.78
68	2	1	-740		-6.36	2.78
69	2	1	-1080	-10.6		3.94
70	2	1	-860		-9.45	3.94
71	2	1	-1560	-15.0		5.13
72	2	1	-1120		-12.7	5.13
73	3	1.015	-1540	-15.2		6.16
74	3	1.015	-1240		-13.6	6.16
75	3	1.015	-1420	-14.5		7.31
76	3	1.015	-1340		-14.1	7.31
77	5	1.010	-1410	-14.7		9.38
78	5	1.010	-1450		-14.9	9.38
79	5	1.010	-1600	-16.1		12.38
80	5	1.010	-1450		-15.4	12.38

---

* Odd numbered gages were installed in meridional direction, and even numbered gages were installed in circumferential direction.

** Distance from centerline of port to center of strain gage, measured along convex surface of hemisphere.

TABLE 6. STRAIN GAGE DATA AND RESULTS FOR ADDITIONAL GAGES AT PORT BOUNDARY, CONFIGURATION A

Strain Gage Number*	Strain Gage Type	Correction Factor, CF	Corrected Strain, ϵ, μ-in./in. (at p = 1500 psi)	Meridional Stress per Unit Load, $\frac{\sigma_m}{p}$, $\frac{psi}{psi}$	Hoop Stress per Unit Load, $\frac{\sigma_h}{p}$, $\frac{psi}{psi}$	Distance**, x, inches	Surface Location	Angular Location, θ, degrees
81	1	1.114	512	-		1.63	Convex	45
82	1	1.114	-		-	1.63	Convex	45
83	1	1.114	-	-		0.63	Concave	45
84	1	1.114	-1110		-	0.63	Concave	45
93	5	1.010	-182	-4.81		0.63	Concave	180
94	5	1.010	-1350		-11.0	0.63	Concave	180
95	5	1.010	71	-2.92		0.63	Concave	270
96	5	1.010	-1350		-10.3	0.63	Concave	270
105	5	1.010	384	-0.31		1.63	Convex	180
106	5	1.010	-1280		-8.98	1.63	Convex	180
107	5	1.010	399	0.17		1.63	Convex	270
108	5	1.010	-1140		-7.84	1.63	Convex	270

---

* Odd numbered gages were installed in meridional direction, and even numbered gages were installed in circumferential direction.

** Distance from centerline of port to center of strain gage, measured along concave or convex surface of hemisphere.

TABLE 7. STRAIN GAGE DATA AND RESULTS, CONFIGURATION A, RERUNS

Strain Gage Number*	Strain Gage Type	Correction Factor, CF	Corrected Strain, ϵ, μ-in. /in. (at p = 1500 psi)	Meridional Stress per Unit Load, $\frac{\sigma_m}{p}$, $\frac{\text{psi}}{\text{psi}}$	Hoop Stress per Unit Load, $\frac{\sigma_h}{p}$, $\frac{\text{psi}}{\text{psi}}$	Distance**, x, inches	Surface Location	Angular Location, θ, degrees
3	1	1.114	106	-2.78		0.63	Concave	0
4	1	1.114	-1400		-10.6	0.63	Concave	0
5	2	1	-925	-9.75		1.50	Concave	0
6	2	1	-1000		-10.1	1.50	Concave	0
7	2	1	-1220	-12.2		2.59	Concave	0
8	2	1	-1070		-11.4	2.59	Concave	0
21	5	1.010	-1690	-0.79		0	Convex	0
22	5	1.010	-1640		-0.78	0	Convex	0
25	1	1.114	-	-		1.63	Convex	0
26	1	1.114	-1280		-	1.63	Convex	0
27	2	1	-225	-3.64		2.78	Convex	0
28	2	1	-740		-6.32	2.78	Convex	0
43	1	1.114	111	-2.68		0.63	Concave	90
44	1	1.114	-1380		-10.4	0.63	Concave	90
45	2	1	-960	-10.1		1.50	Concave	90
46	2	1	-1030		-10.5	1.50	Concave	90
47	2	1	-1270	-12.6		2.59	Concave	90
48	2	1	-1090		-11.7	2.59	Concave	90
65	1	1.114	356	-0.61		1.63	Convex	90
66	1	1.114	-1320		-9.34	1.63	Convex	90
67	2	1	-245	-3.83		2.78	Convex	90
68	2	1	-750		-6.45	2.78	Convex	90
81	1	1.114	356	-		1.63	Convex	45
82	1	1.114	-		-	1.63	Convex	45
83	1	1.114	111	-2.10		0.63	Concave	45
84	1	1.114	-1160		-8.71	0.63	Concave	45

---

* Odd numbered gages were installed in meridional direction, and even numbered gages were installed in circumferential direction.

** Distance from centerline of port to center of strain gage, measured along concave or convex surface of hemisphere.

TABLE 8. STRAIN GAGE DATA AND RESULTS, CONFIGURATION B, θ = 0°

Strain Gage Number*	Strain Gage Type	Correction Factor, CF	Corrected Strain, ϵ, μ-in./in. (at p = 1500 psi)	Meridional Stress per Unit Load, $\frac{\sigma_m}{p}$, $\frac{psi}{psi}$	Hoop Stress per Unit Load, $\frac{\sigma_h}{p}$, $\frac{psi}{psi}$	Distance**, x, inches	Surface Location
7	2	1	-1260	-12.6		2.59	Concave
8	2	1	-1100		-11.7	2.59	Concave
9	2	1	-1340	-13.5		3.69	Concave
10	2	1	-1200		-12.7	3.69	Concave
11	2	1	-1610	-15.9		4.75	Concave
12	2	1	-1340		-14.6	4.75	Concave
13	3	1.015	-1510	-15.4		5.78	Concave
14	3	1.015	-1430		-15.0	5.78	Concave
15	3	1.015	-1470	-15.2		6.81	Concave
16	3	1.015	-1460		-15.1	6.81	Concave
17	4	0.985	-1470	-15.5		8.81	Concave
18	4	0.985	-1590		-16.1	8.81	Concave
19	4	0.985	-1320	-14.3		11.69	Concave
20	4	0.985	-1580		-15.6	11.69	Concave
31	2	1	-1500	-14.6		5.13	Convex
32	2	1	-1140		-12.7	5.13	Convex
33	3	1.015	-1480	-14.7		6.16	Convex
34	3	1.015	-1270		-13.7	6.16	Convex
35	3	1.015	-1380	-14.2		7.31	Convex
36	3	1.015	-1360		-14.1	7.31	Convex
37	4	0.985	-1420	-14.7		9.38	Convex
38	4	0.985	-1420		-14.7	9.38	Convex
39	4	0.985	-1440	-15.0		12.38	Convex
40	5	1.010	-1470		-15.1	12.38	Convex
115	7	1.015	-715	-8.14		1.50	Concave
116	6	0.985	-1010		-9.67	1.50	Concave
125	7	1.015	-235	-4.05		2.78	Convex
126	6	0.985	-867		-7.34	2.78	Convex
127	7	1.015	-1070	-10.7		3.94	Convex
128	6	0.985	-946		-10.1	3.94	Convex

---

* Odd numbered gages were installed in meridional direction, and even numbered gages were installed in circumferential direction.

** Distance from centerline of port to center of strain gage, measured along concave or convex surface of hemisphere.

TABLE 9. STRAIN GAGE DATA AND RESULTS, CONFIGURATION B, $\theta = 90°$

Strain Gage Number*	Strain Gage Type	Correction Factor, CF	Corrected Strain, ϵ, μ-in./in. (at p = 1500 psi)	Meridional Stress per Unit Load, $\frac{\sigma_m}{p}$, $\frac{psi}{psi}$	Hoop Stress per Unit Load, $\frac{\sigma_h}{p}$, $\frac{psi}{psi}$	Distance**, x, inches	Surface Location
47	2	1	-1340	-13.0		2.59	Concave
48	2	1	-1040		-11.5	2.59	Concave
49	2	1	-1380	-		3.69	Concave
50	2	1	-		-	3.69	Concave
51	3	1.015	-1620	-16.0		4.75	Concave
52	3	1.015	-1320		-14.4	4.75	Concave
53	3	1.015	-1540	-15.6		5.78	Concave
54	3	1.015	-1430		-15.1	5.78	Concave
55	3	1.015	-1520	-15.6		6.81	Concave
56	3	1.015	-1480		-15.4	6.81	Concave
57	3	1.015	-1560	-16.0		8.81	Concave
58	3	1.015	-1530		-15.9	8.81	Concave
59	5	1.010	-1490	-15.6		11.69	Concave
60	5	1.010	-1600		-16.2	11.69	Concave
73	3	1.015	-1510	-14.9		6.16	Convex
74	3	1.015	-1240		-13.5	6.16	Convex
77	5	1.010	-1450	-14.9		9.38	Convex
78	5	1.010	-1410		-14.7	9.38	Convex

---

* Odd numbered gages were installed in meridional direction, and even numbered gages were installed in circumferential direction.

** Distance from centerline of port to center of strain gage, measured along concave and convex surface of hemisphere.

TABLE 10. STRAIN GAGE DATA AND RESULTS FOR GAGES AT PORT BOUNDARY, CONFIGURATION B

Strain Gage Number*	Strain Gage Type	Correction Factor, CF	Corrected Strain, ϵ, μ-in. /in. (at p = 1500 psi)	Meridional Stress per Unit Load, $\frac{\sigma_m}{p}$, $\frac{psi}{psi}$	Hoop Stress per Unit Load, $\frac{\sigma_h}{p}$, $\frac{psi}{psi}$	Distance**, x, inches	Surface Location	Angular Location, θ, degrees
111	7	1.015	682	1.36		0.76	Concave	0
112	6	0.985	-1540		-10.2	0.76	Concave	0
113	7	1.015	520	0.56		0.76	Concave	90
114	6	0.985	-1360		-9.20	0.76	Concave	90
121	7	1.015	536	0.32		1.77	Convex	0
122	6	0.985	-1500		-10.3	1.77	Convex	0
123	7	1.015	406	-1.13		1.77	Convex	90
124	6	0.985	-1670		-11.9	1.77	Convex	90

---

* Odd numbered gages were installed in meridional direction, and even numbered gages were installed in circumferential direction.

** Distance from centerline of port to center of strain gage, measured along concave and convex surface of hemisphere.

TABLE 11. STRAIN GAGE DATA AND RESULTS FOR GAGES AT BOUNDARIES OF CABLE PENETRATIONS WITHOUT BOLT HOLES, CONFIGURATION B

Strain Gage Number*	Strain Gage Type	Correction Factor, CF	Corrected Strain, ϵ, μ-in./in. (at p = 1500 psi)	Boundary Stress per Unit Load, $\frac{\sigma_b}{p}$, $\frac{\text{psi}}{\text{psi}}$	Distance from Edge of Hole, inch
Gages around 0.358" Diameter Cable Penetration without Bolt Holes					
211	6	0.985	-2380	-16.5	0.05
212	6	0.985	-1360	-9.39	0.06
213	6	0.985	-2740	-19.0	0.04
214	6	0.985	-1090	-7.54	0.06
215	6	0.985	-2470	-17.2	0.05
216	6	0.985	-1540	-10.7	0.05
Gages around 0.144" Diameter Cable Penetration without Bolt Holes					
241	6	0.985	-1420	-9.83	0.12
242	6	0.985	-1090	-7.54	0.06
243	6	0.985	-2080	-14.4	0.04
245	6	0.985	-1620	-11.2	0.10
246	6	0.985	-1190	-8.25	0.05

---

* Odd numbered gages were located on concave surface, and even numbered gages were located on convex surface.

TABLE 12. STRAIN GAGE DATA AND RESULTS FOR GAGES AT BOUNDARIES OF CABLE PENETRATIONS AND BOLT HOLES, CONFIGURATION B

Strain Gage Number*	Strain Gage Type	Correction Factor, CF	Corrected Strain, ϵ, μ = in./in. (at p = 1500 psi)	Boundary Stress per Unit Load, $\frac{\sigma_b}{p}$, $\frac{psi}{psi}$	Distance from Edge of Hole, inch
Gages around 0.358" Diameter Cable Penetration with Bolt Holes					
221	6	0.985	-2310	-16.0	0.07
222	6	0.985	-1250	-8.63	0.08
223	6	0.985	-2600	-18.0	0.04
224	6	0.985	-1020	-7.10	0.04
225	6	0.985	-2310	-16.00	0.05
226	6	0.985	-1830	-12.7	0.10
227	6	0.985	-2300	-16.0	0.05
Gages around 0.109" Diameter Bolt Holes near 0.358" Diameter Cable Penetration					
232	6	0.985	-827	-5.73	0.04
234	6	0.985	-732	-5.08	0.03
236	6	0.985	-1470	-10.2	0.04
238	6	0.985	-1430	-9.94	0.04
Gages around 0.144" Diameter Cable Penetration with Bolt Holes					
251	6	0.985	-1770	-12.2	0.05
252	6	0.985	-1100	-7.65	0.05
253	6	0.985	-2220	-15.4	0.06
254	6	0.985	-772	-5.35	0.05
255	6	0.985	-1650	-11.5	0.06
256	6	0.985	-1300	-9.01	0.06
Gages around 0.109" Diameter Bolt Holes Near 0.144" Diameter Cable Penetration					
262	6	0.985	-827	-5.73	0.03
264	6	0.985	-749	-5.19	0.04

---

* Odd numbered gages were located on concave surface, and even numbered gages were located on convex surface.

APPENDIX A

EPISTEMOLOGY OF BIREFRINGENT COATING TECHNIQUE

1. History of the Birefringent Coating Technique

The birefringent coating technique of experimental stress analysis was originated by Mesnager(7) in France, 1930. He was the first to suggest bonding a photoelastic material to a polished surface and then relate the strains in the coating to the surface strains of the structure.

Mabboux(8) in France, 1932, suggested using heterogeneous inclusions of photoelastic material in concrete structures, and using a Nörrenberg doubler to measure the stress. This arrangement has few applications, since the inclusion merely acts as a single strain gage.

Oppel(9) in Germany, 1937, determined notch stresses with a birefringent coating. The plastic which he used, however, was not sufficiently sensitive optically for general applications.

D'Agostino(10) and colleagues of the United States reported a birefringent coating technique in 1954. Their results, however, were applicable only for flat parts.

Zandman, while in France, discovered an epoxy formula and reported in 1953 that the plastic could be used satisfactorily on a practical basis for elastic or plastic ranges and for any size or shape. The Zandman method(11) has been used widely in Europe and was introduced in the United

States in 1956. The plastic which Zandman discovered is now referred to as Photostress and is commercially available from the Budd Company.

2. Principles of the Birefringent Coating Analysis

Birefringent coatings combine the functions of photoelasticity, brittle lacquer, and electric resistance strain gages. The birefringent coating is analogous to an infinite number of strain gages, since the strain is identified by the contrast of colors.

Basically, birefringent coating principles are the same as in photoelasticity. The mathematical formulas expressing the fundamental relationships used in photoelasticity analysis have been thoroughly developed in the literature(12, 13, 14) and will not be reiterated here.

The primary difference between photoelasticity and the birefringent coating analysis is that a transparent model, such as glass or plastic, is utilized in photoelasticity, whereas the actual structure is tested in a birefringent coating analysis. When a transparent coating is applied to a structure, the coating follows the surface strains of the structure. With applied load, the coating exhibits a relative retardation of polarized light proportional to the strain because of the doubly refractive, or birefringent, characteristic of the coating. Since the light waves are polarized at 90° to each other, corresponding to the principal stress directions, only the difference of principal stresses is obtained with normal incidence. Fortunately, there are several means of determining the individual principal stresses.

The isostatics, the principal stress trajectories, can be readily obtained from the isoclinics, the locus of points along which the principal stresses have parallel directions. The whole field isostatics are determined by rotating the analyzer with respect to the polarizer in a plane polariscope, usually using white light.

A common procedure for determining the individual principal stresses is by first determining the isopachics, the sum of the principal stresses. Knowing the isopachic and the isochromatic, the principal stress difference, at a point, the individual principal stresses can then be readily calculated.

Another method for determining the individual principal stresses is by integrating Filon's transformations of the Lamé-Maxwell equations, as illustrated in Reference 13, page 287. The principal stress at a boundary equals the isochromatic, since the other principal stress, perpendicular to and at the boundary, is zero in a plane stress problem. From a consideration of the boundary stresses, the isoclinics, and the isochromatics, an approximate solution may then by obtained by graphical integration. Other means sometimes used for determining the individual principal stresses is the shear difference method and the slope equilibrium method, as illustrated in Reference 13, pages 215 and 270, respectively.

The method most commonly used for determining the individual principal stresses is by the consideration of oblique incidence(15, 16). Mathematical relationships exist for finding the principal stresses from normal and oblique incidence measurements of relative retardation.

The shear stresses in a structure can be fairly accurately determined by visual observation of the birefringent coating and utilizing a strain-stress color chart(17). A method commonly used to more accurately determine whole field shear stresses is the Tardy Method(18) (goniometric compensation), which utilizes fringe shift from analyzer rotation. Beginning with a dark field circular polariscope, which has crossed polarizers and crossed quarter wave plates or parallel polarizers and parallel quarter wave plates, rotating the analyzer 90° causes the fringes to shift to a light field, and an additional 90° rotation in the same direction causes the fringes to shift further to a dark field again. Knowing the fringe constant, f, the stress at some point between adjacent fringes can then be determined within an accuracy of f/180.

Fringe multiplication(19, 20, 21) is another method useful in determining whole field shear stresses. This technique has been successfully used in experimental work with birefringent coatings, but the limitations are in-plane loading and studies of flat surfaces. The surface area being studied has to have a specular finish and be optically flat, but this can be easily achieved by various electropolish or electroplating procedures. With a system of mirrors, the number of fringes can be increased as many as five times, dependent upon the quality of the specimen surface.

The Babinet Compensator is a means of adding a known birefringence, since the compensator is a calibrated quartz wedge which is optically flat on each side. The compensator constant is the number of divisions between

successive tints of passage, usually considered as the sharp distinction between the erubescent and blue colors.

The difference in wedge thickness for the number of divisions corresponding to the compensator constant is one wave-length of white light, 22.7×10^{-6} inches. For an incremental change of load on the specimen, the tint of passage moves along the compensator. The number of divisions that the tint of passage moves on the compensator is the figure used in the stress computations.

3. Advantages of a Birefringent Coating Analysis

The technique of birefringent coating analysis is useful in determining:

a. The elastic or plastic strain distribution from static or dynamic loading.

b. Instantaneous detection of stress concentration areas.

c. Stress concentration factors around cracks, small holes, fillets, and notches(22).

d. Residual strains or stress from plastic deformations.

e. True Yield strength.

f. Stresses in composite materials such as reinforced concrete.

g. Stresses in anisotropic materials such as wood.

h. Stresses in and around the weld of dissimilar metals.

i. Stresses in and around heterogeneous inclusions(19).

Some of the special advantages of birefringent coating analysis are as follows:

a. The size of the specimen can vary from a small crystalline grain to very large structures.

b. The tests can be telemetered.

c. Measurements can be automated by means of photocells and servo-mechanisms.

d. An analysis can be made in almost any atmospheric condition.

e. An analysis can be made with the specimen completely submersed in any transparent liquid such as water or oil.

f. With normal incidence readings, the strain (or stress) is obtained at a point rather than over a finite gage length.

g. The individual principal stresses at a point can be obtained with great accuracy from normal and oblique incidence readings if the specimen is symmetrical.

h. If a specimen is not symmetrical, the integrating effect due to gage length can be varied when the individual principal stresses are to be obtained.

i. The strains (or stresses) can be obtained exactly at the edge of free boundaries(15, 16).